The formation of PAHs and soot platelets: Multiconfiguration theoretical study of the key step in the Ring closure-Radical breeding polyyne-based mechanism

UNIVERSITÀ DEGLI STUDI DI TORINO

The Formation of PAHs and Soot Platelets: Multiconfiguration Theoretical Study of the Key Step in the *Ring Closure-Radical Breeding* Polyyne-based Mechanism.

Antonius Indarto, Anna Giordana, Giovanni Ghigo, and Glauco Tonachini*

Dipartimento di Chimica Generale e Chimica Organica, Università di Torino, Corso Massimo D'Azeglio 48, I-10125 Torino, Italy

Polyynes, of general formula H–(C≡C–)$_n$H, are known to play a significant role in combustion and pyrolysis, possibly being intermediates in the formation of polycyclic aromatic hydrocarbons (PAHs) and soot. They have also been detected in astrophysical investigations. The key step in the polyyne-based *radical breeding* mechanism for PAH growth, put forward by Krestinin, is a cyclization that implies disruption of electron couples, hence plausibly expected to be energy demanding. We explore by quantum mechanical multiconfiguration methods (CASSCF and CASPT2) the electronic features and energy requirements of such a process in itself. The wavefunction features are analyzed, and free energy barriers estimated over a wide range of temperatures, for three molecular models. The initial radical adduct A, generated by H$^{\bullet}$, HC≡C$^{\bullet}$ (ethynyl), or HC≡C–C$^{\bullet}$H$_2$ (propargyl) addition to butadiyne (HC≡C–C≡CH), undergoes a cyclization with generation of two new radical centers. However, in most cases, one of these new singly occupied sp^2 orbitals has some overlap with the unpaired electron lobe already existent in A: some sort of bonding builds up and the triradical character cannot consequently be large. Only one model suggests a possible role of the radical breeding mechanism during combustion. (190 words)

- keywords: 1 "polycyclic aromatic hydrocarbons", 2 "PAH/soot formation", 3 "radical breeding mechanism", 4 polyynes, 5 cyclization
- running title: "*PAH Formation: Radical Breeding Polyyne Mechanism*"
- short title: "PAH and Soot Formation: the *Radical Breeding* Polyyne Mechanism"
- graphical abstract for the *graphical table of contents*:

The key step in the polyyne-based radical breeding mechanism for PAH growth is a cyclization with disruption of electron couples, plausibly expected to be energy demanding. For such a process, the wavefunction features are analyzed, and free energy barriers are estimated over a wide range of temperatures. (48 words)	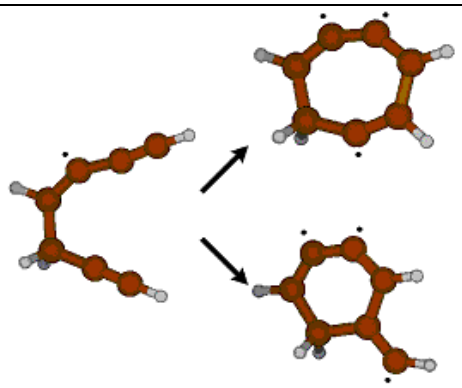	**The Formation of PAHs and Soot Platelets: Multiconfiguration Theoretical Study of the Key Step in the *Ring Closure-Radical Breeding* Polyyne-based Mechanism.** Antonius Indarto, Anna Giordana, Giovanni Ghigo, and Glauco Tonachini

* e-mail: glauco.tonachini@unito.it - phone ++39-011-6707648 - fax: ++39-011-2367648

INTRODUCTION

Polycyclic aromatic hydrocarbons (PAHs) and soot particles are important components of the variety of organic pollutants present in the earth troposphere.[1] Soot shares the same nature and origin of PAHs and can be found in association with them. It has in fact an irregular agglomerate structure of graphenic layers, which can be curved and present defects, clustered in globular particles, whose size is ca. 10-80 nm.[2] Their actual composition and morphology depend on the source and combustion/pyrolysis conditions.[3] Polycyclic aromatic hydrocarbons and soot platelets are generated in the same combustion processes at relatively low O_2 concentrations,[4] or under pyrolysis conditions.[3,5] The study of their formation mechanism and growth kinetics is of current interest, and is carried out both experimentally and by kinetic simulations.[6] However, PAHs and PAH cations, PAH clusters, and amorphous carbon clusters have also been identified (to some extent tentatively) out of the terrestrial environment, namely in planetary atmospheres[7] as well as in the envelopes of carbon-rich stars[8] or in the interstellar medium,[9] hence under a wide variety of pressure and temperature conditions. Therefore, clarifying the PAH growth mechanism is important not only for a better knowledge of combustion or pyrolysis chemistry[10] but also in astrophysical investigations on the atmospheres of the solar system planets,[7] or on carbon-rich stellar outflows.[11]

The most commonly mentioned and discussed growth mechanism for PAHs and soot particles, under combustion conditions, is the *HACA* mechanism (*H*ydrogen *A*bstraction – C_2H_2 *A*ddition), independently proposed by Frenklach[12] and Bockhorn,[13] which involves alternate cyclization and ethyne addition steps. Some variants, such as that put forward by Bittner and Howard,[14] have been discussed in more recent years,[9,15] also within gas-phase quantum mechanical studies.[16,17,18] Also other mechanisms have been considered possible or promising,[19] as the fast polymerization of polyynes, proposed by Krestinin,[20] whose key step is investigated in this study. Polyynes have been found to be present in significant amounts in flames,[4] as well as in the interstellar medium.[21] They have also been detected as main products in radical reactions carried out at room temperature, and their formation discussed in connection with the chemistry of Titan's atmosphere.[22] Recently, special focus on polyynes in flames has been put in two experimental studies, in which they have been detected either up to $C_{10}H_2$,[23] or to $C_{12}H_2$, with a concentration ratio $C_{2n}H_2/C_{2(n-1)}H_2$ which results almost constant.[24] Central to Krestinin's hypothesis is the proliferation of radical centers (*breeding*), which should accompany cyclization processes taking place within a polyyne fast polymerization process. The polyyne mechanism has been taken into account in recent years within photochemical/ kinetic modeling schemes.[25]

This study is focused on assessing the electronic features and the energy requirements of the **ring formation–radical breeding** step in itself, for some molecular models. With this purpose, we will examine some radical proliferation steps which take place upon cyclization of a radical adduct. Three molecular systems are chosen (Models 1-3), by imagining the attack of a radical initiator $X^{\bullet}$, namely just $H^{\bullet}$ (1), or ethynyl, $HC{\equiv}C^{\bullet}$ (2), or propargyl, $HC{\equiv}C{-}C^{\bullet}H_2$ (3), onto butadiyne (also called diacetylene, $HC{\equiv}C{-}C{\equiv}CH$), or hexatriyne, $HC{\equiv}C{-}C{\equiv}C{-}C{\equiv}CH$. In the first model, the radical intermediate obtained by hydrogen addition attacks in turn another closed-shell unsaturated molecule, and gives a radical adduct, which subsequently undergoes cyclization. In the other two models, the first radical intermediate cyclizes. The proliferation of radical centers is attained, in all cases, in the cyclization step, with formation of two new radical centers. All reaction schemes involve, as substrate, the butadiyne molecule, which has been detected as an important intermediate in rich sooting flames.[24,26,27,28] This role has also prompted the experimental study of its pyrolysis.[29] Its concentration, as well as those of ethyne, propargyl, and hexatriyne (among many others),[30] has been recently determined in flames of ethyne,[24] benzene,[26] or gasoline.[27]

THEORETICAL METHODS

Multiconfigurational quantum mechanical calculations were carried out for Models 1-3. This approach is the most suitable when chemical events involving the disruption of electron couples and/or the formation of di- or poly-radical species are considered, and allows a useful analysis of the wavefunction traits.

Stable and transition structures (TS), relevant to the radical site proliferation step, were optimized within the Complete Active Space (CAS) variant of the Multi-Configuration Self Consistent Field (MCSCF) theory (CASSCF, for short).[31] All optimized geometries are collected as cartesian coordinates in the Supplemental Material, pp 1-9. The active space was chosen by a uniform criterion for all models, in the sense that it encompasses all the orbitals that lie on the molecular plane and are involved in bond and unpaired electron formation upon cyclization of the adduct A. Thus, for all models, the space defined to discuss the features of the cyclization-radical center proliferation step can be labeled as (5,5), meaning 5 electrons in 5 active orbitals: in A, two in-plane π bonds (i.e. two π, π^* MO couples) plus one unpaired electron in a ca. sp^2 hybrid, which become, upon cyclization, one σ bond (i.e. one σ, σ^* MO couple) plus three unpaired electrons in ca. sp^2 hybrids. A validation of this choice is presented in the Appendix. Schematic details of the chosen active MOs are presented below in Schemes 3, 6, and 8.[32a] Actual plots[32b] of them are presented in the Supplemental Material for the transition structures, pp 9-16. Since in the next Section some comparisons will be drawn with the Bergman reaction (vide infra), we specify here that the active space encompasses in that

case the same MOs as in models 1-3, minus the initial sp^2 hybrid associated to the unpaired electron of the starting radicals, since the Bergman "reactant" is a closed shell molecule. Hence a (4,4) CAS results.

A vibrational analysis was carried out at the CASSCF level in correspondence of each critical point. The basis set used in this phase is Dunning's cc-pvTZ.[33a] Energies were then reassessed by taking into account dynamic correlation at the CASPT2[34] level, with the standard IPEA shifted $\hat{H}_0$ operator,[35] developed for a correct calculation of the correlation energy in open shell systems. These single-point energy calculations were carried out with the cc-pvTZ basis set, and also with the more extended cc-pvQZ.[33b] This allowed us to extrapolate to the complete basis set (CBS) limit, by exploiting the extrapolation formula proposed by Halkier *et al*.[36] All total energies are collected in the Supplemental Material, pp 1-9, for each critical point. Finally, the CASPT2/CBS energies (first column under the heading ΔE in the Tables 1, 4, and 6) were combined with the thermochemistry[37] computed at the CASSCF level[31b] to roughly estimate Gibbs "free energy differences" for different temperatures (columns under the heading "ΔG" in the Tables 1, 4, and 6). In one case there was indication that the CASPT2 maximum was shifted with respect to the CASSCF TS. The surface was then probed by constrained optimizations in order to define a CASPT2 profile.

The structure optimizations and vibrational analyses were carried out with the program Gaussian 03.[31b,38] The CASPT2 calculations were performed by using the MolCAS 7.2 program.[39,40]

RESULTS AND DISCUSSION

Tables 1, 4, and 6 report the energetics for the reacting systems chosen to model the radical breeding mechanism: ΔE and ΔG, in kcal mol^{-1}, for different temperatures (T reported in Kelvin degrees). The radical addition plus cyclization model reactions are shown in Schemes 1, 5, and 7. Given that the focus is on the cyclization/radical proliferation step in itself, the adduct that undergoes cyclization is taken as the reference energy level, and is labeled "A", while the cyclized "product" is labeled "B". The schemes can be compared with those originally propounded by Krestinin.[20] Tables 2, 5, and 7 report, for two wavefunction features, a comparison of the step A-B in the three models with respect to the equivalent step in the Bergman reaction (Table 3) .

Model 1. The linear HC≡C–C≡CH system (butadiyne, BD) gets bent to some extent upon initial H· addition to a terminal carbon. The resulting adduct **1** (Scheme 1) still carries one unpaired electron, by which it can add to another BD molecule and give **2**, which is the initial reference adduct A in this case. The adduct **2** still carries only one unpaired electron, of course, but a proliferation of radical centers could take place upon cyclization. The intermediate **3**,

containing a six-membered ring (6-ring), and carrying three unpaired electrons, could form through path **a**. The CASPT2/CBS energy difference between the ground state doublet and the corresponding quartet[41] in **3** is 4.7 kcal mol^{-1}. This value is consistent with the geometric arrangement in **3**, where the lobes carrying a single electron are far apart. This scheme is very close to the original Krestinin's scheme.[20] Actually, the step is significantly endoergic (Figure 1). The para-quinoid structure **3** cannot imply a significant energy gain, in front of the destabilization brought about by the net disruption of one electron pair. The ΔG variation with T is moderate.

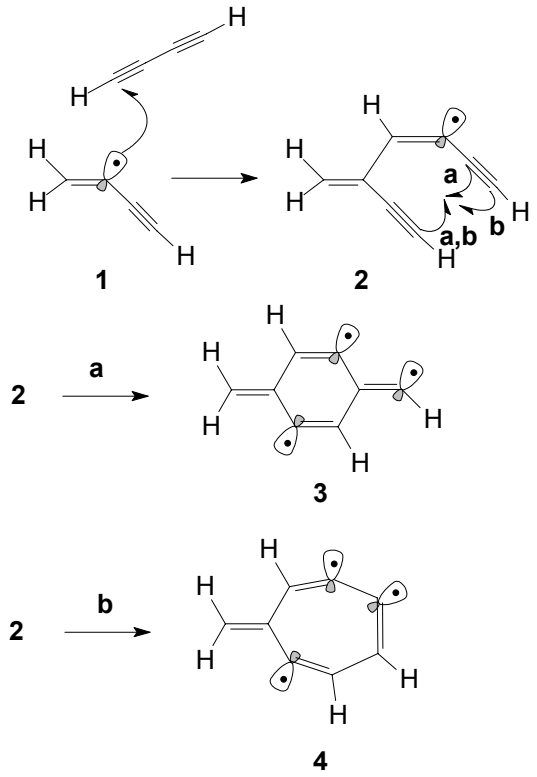

Scheme 1. Model system 1 (H + butadiyne, then + butadiyne again) of the radical center proliferation mechanism for PAH growth (see Table 1).

TABLE 1. Model system 1: CASPT2/CBS energy[a] and "free energy" [b] differences.

	ΔE	ΔG /kcal mol^{-1}					
T/K:		*900*	*1200*	*1500*	*1800*	*2100*	*2400*
add. TS **1**-**2**	44.8	35.1	32.8	30.6	28.5	26.5	24.5
2 (A)	0.0	0.0	0.0	0.0	0.0	0.0	0.0
TS **2**-**3**	34.1	44.4	48.6	53.0	57.6	62.2	66.9
	36.3	*46.6*	*50.8*	*55.3*	*59.8*	*64.4*	*69.1*
3	36.1	49.0	53.3	57.7	62.1	66.4	70.8
TS **2**-**4**	27.3	35.9	39.7	43.6	47.6	51.8	56.0
4	-1.0	13.4	18.1	22.9	27.6	32.4	37.2

[a]values in italic: point of maximum E for a CASPT2 scan (see Method section).
[b]CASPT2/CBS energies combined with CASSCF/cc-pvTZ vibrational analysis.

A competitive 7-ring closure of **2** to **4** (path **b**) would similarly bring about an increment of the number of radical centers. The *G* barrier for step **2**-**4** is lower than for **2**-**3**, by 8.5–11 kcal mol^{-1}, and the step less endoergic, at any T. But, in this case, that a genuine proliferation of radical centers had taken place can be seen as questionable. Indeed, two radical lobes are adjacent, as in *o*-benzyne. A significant overlap is present between the two radical lobes, and the CASPT2/CBS energy difference between the ground state doublet and the corresponding quartet[41] in **4** (49.2 kcal mol^{-1}) indicates that some bonding is present. However, an *o*-benzyne-like structure has to be reactive too (usually, though not necessarily, via cycloaddition reactions).[42]

The steps **2**-**3** and **2**-**4** of Scheme 1 recall the Bergman reaction (Z-hex-3-ene-1,5-diyne to *p*-benzyne conversion: Scheme 2).[43] This cyclization process is archetypal for cyclization processes that can bring about the formation of radical centers. Since it implies the net disruption of one electron couple (*p*-benzyne has diradical character), though balanced to some extent by the formation of an aromatic ring, this step is in itself rather energy-demanding.[44]

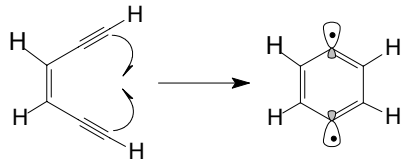

Scheme 2. The Bergman reaction.

The main difference with our models **1**-**3** here (see also structures **5**-**9** below) is the substitution of one C–H bond with an unpaired electron in both the open-chain intermediates A and the cyclic “products” B. The Bergman reaction was investigated in the past years at different levels of theory, among which we can mention a coupled cluster study by Kraka and Cremer,[45] a CASSCF-CASPT2 study by Lindh et al.[46] and, more recently, a thorough study of the performances of DFT, using seven functionals and four basis sets.[47]

Two wavefunction features are chosen in the following to discuss the nature of the ring closure process. The first one is the electron population of the active orbitals. The second one is the relative importance of the principal electron configurations (CF), expressed by the CI coefficients (c_i) in the CAS multiconfiguration wave-function Ψ. Let us first begin by defining the nature of the five active orbitals. In Scheme 3 (as in the following Schemes 6 and 8) these are sketched[32a] for “reactant” **2** and “products” **3** and **4**. It is to be intended that actual MO plots[32b] see a significant mixing and polarization of these schematic contributions and appear consequently more delocalized. They can be found for all transition structures in the Supplemental Material (when inspecting these, the reader can observe that they “keep memory” of the interacting π, π^* couples of the reagents, while hinting at the same time at the forming σ, σ^* couples of the products). The orbitals in the Schemes 3, 6, and 8 are presented in the same order as in the pertinent Tables 2, 5, and 7, respectively, and are characterized as

follows for Model 1, similarly for the other two models. "Reactant": (1) and (2) are those originating from the combinations of the in-plane π orbitals; (4) and (5) are the related antibonding combinations; (3) is associated to the unpaired electron. On the "products" side we find: on one hand, the σ, σ* orbitals pertinent to the new σ bond, (1) and (5); on the other hand the two sp^2 hybrids associated to electrons unpaired only to some degree (see the above discussion), which consequently appear as in-phase and out-of-phase combinations, plus (3) one sp^2 hybrid associated to one unpaired electron (γ_i values in italic).

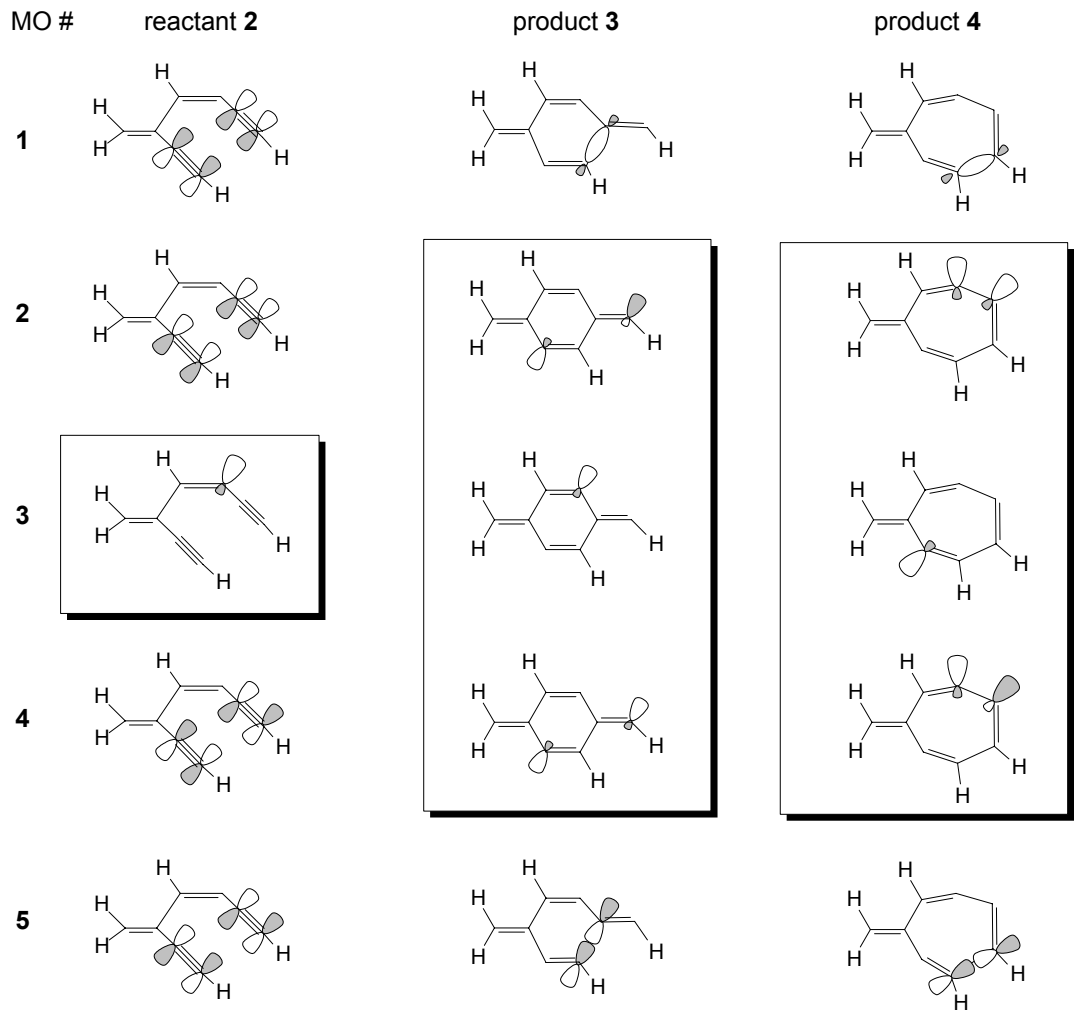

Scheme 3. Active orbitals for Model system 1. Boxes collect orbitals with occupations more or less appreciably from 2 or 0 (compare data in Table 2), related to the presence of unpaired electrons.

Table 2 reports the relevant data for the step A-B in Model 1, which can be compared to the equivalent step in the Bergman reaction (Table 3). Scrutiny of these data shows (bold figures draw attention onto some values commented in the text) that, proceeding from TS **2**-**3** to **3**, some increasing diradical character is witnessed by two active-MO populations (γ_i: 1.59-1.30 and 0.40-0.70), and by a decreasing weight of the most important configuration in Ψ (c_i= 0.85-0.76).[48] These traits are in accord with the small energy difference between the doublet and the quartet mentioned above.

TABLE 2. Wavefunction features for the ring closure step in model system 1.

	2	TS **2-3**	**3**	TS **2-4**	**4**
Active MO #	One-electron symbolic density matrix diagonal elements γ_i				
1	1.945	1.954	1.983	1.922	1.985
2	1.931	**1.593**	**1.300**	**1.826**	**1.859**
3	*1.001*	*1.004*	*1.002*	*1.002*	*1.000*
4	0.068	**0.404**	**0.697**	**0.172**	**0.141**
5	0.056	0.045	0.017	0.076	0.015
CF		Largest CAS(5,5)[a] CI coefficients:[b]			
$\mathbf{1^2\ 2^2\ 3^1}$	0.961	**0.854**	**0.764**	0.912	0.960
$\mathbf{1^2\ 3^1\ 4^2}$		0.371	0.531		0.264
$\mathbf{2^2\ 3^1\ 5^2}$	0.152				
$\mathbf{1^2\ 2^1\ 3^1\ 4^1}$		-0.247	-0.273	0.214	
$\mathbf{1^2\ 2^1\ 3^1\ 5^1}$				0.177	

[a]active space encompassing one sp^2 hybrid associated to one unpaired electron (γ_i values in italic), plus the "reactant" in-plane π, π^* couples involved in the formation of the "product" σ bond and of the two sp^2 hybrids electron occupations differing more or less significantly from 2 or 0, related to the presence of new "unpaired" electrons (γ_i: bold values). See text and Scheme 3 for details.
[b]values larger than 0.15 reported.

Coming to TS **2-4** and **4**, some diradical character is still present, but to a limited extent, and slightly larger in the TS than in **4** (γ_i: 1.83-1.86 and 0.17-0.14, and c_i= 0.91-0.96, respectively). This is consistent with the fact that the overlap between the two adjacent lobes is significant and results in the substantial doublet – quartet splitting just discussed.

We can compare these traits with the similar structures in the Bergman reaction. There, the (4,4) active space encompasses the "reactant" in-plane π, π^* couples involved in the formation of the "product" new σ bond and of the two orbitals with electron occupations differing significantly from 2 or 0, related to the presence of two new unpaired electrons (Scheme 4). When comparing the structures of Model 1 with the similar structures in the Bergman reaction (Table 3), we see that in the latter a diradical character is evident and grows up in going from the TS to *p*-benzyne (γ_i: 1.70-1.19 and 0.30-0.81), as is expected for the formation of a structure having substantial diradical character. The coefficients of the most important configurations replicate the same trend (c_i= 0.91-0.77).[41,49]

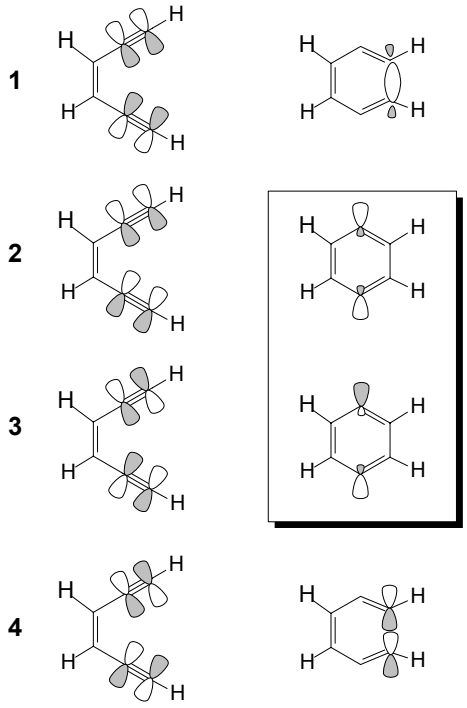

Scheme 4. Active orbitals for the Bergman reaction. Boxes collect orbitals with occupations deviating appreciably from 2 or 0 (compare data in Table 3), related to the presence of unpaired electrons.

TABLE 3. Comparison of the wavefunction features for the ring closure step in the Bergman reaction.

	Hexenediyne	ring closure TS	*p*-benzyne
Active MO #	One-electron symbolic density matrix diagonal elements γ_i		
1	1.942	1.937	1.989
2	1.945	**1.699**	**1.191**
3	0.056	**0.303**	**0.809**
4	0.057	0.060	0.011
CF	Largest CAS(4,4)[a] CI coefficients:[b]		
$\mathbf{1^2\ 2^2}$	0.972	0.906	**0.770**
$\mathbf{1^1\ 2^1\ 3^1\ 4^1}$	0.165	-0.170	
$\mathbf{1^2\ 3^2}$		-0.358	**-0.634**

[a] Active space as in models 1-3, minus the initial sp^2 hybrid associated to the unpaired electron in the starting radicals **2**, **5**, and **7**. See note 50, and the Supplemental Material for further details.
[b] values larger than 0.15 reported.

Model 2. Then, we looked for an alternative, in which the destabilization caused by the unpairing of electrons could be counterbalanced by some stabilizing factor. Thus, the addition of ethynyl (HC≡C▪) to BD (Scheme 5, step a) would bring about the formation of **5** [the same result would be obtained also from H˙ addition to a central position of the HC≡C–C≡C–C≡CH

system, hexatriyne, HT (Scheme 5, step b); this could be a reversible process (-b)]. **5** is our initial adduct A in both cases, and its cyclization gives a doublet triradical **6**, whose six-membered ring carries an aromatic π system (Scheme 2).

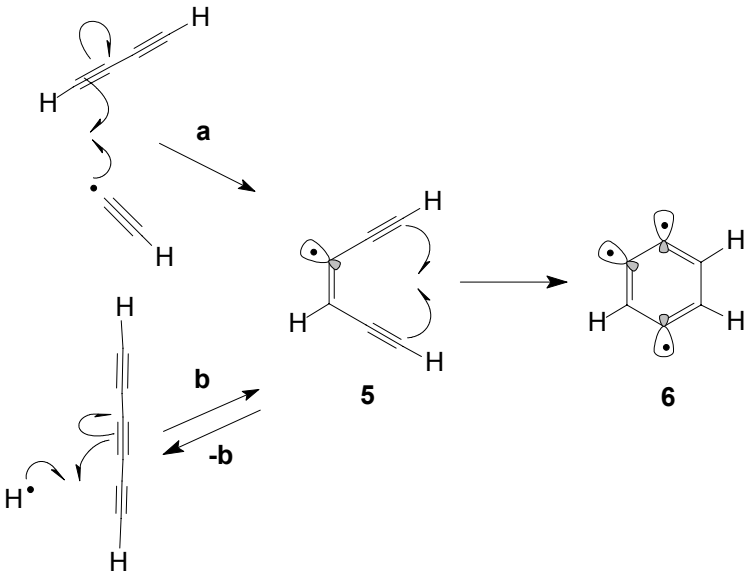

Scheme 5. Model system 2 (ethynyl + butadiyne, BD, or, equivalently, hydrogen atom + hexatriyne, HT) of the radical center proliferation mechanism for PAH growth (see Table 4).

In Table 4 we see barrier values which lie in between those seen for Model 1. They are lower than those for step **2**-**3**, by 5.5–8 kcal mol^{-1}, but slightly higher than those for step **2**-**4**, by ca. 3 kcal mol^{-1}. The temperature dependence is similar (an increase of 22 – 25 kcal mol^{-1}, in going from T = 900 to 2400 K). The step is less endoergic, in particular with respect to **2**-**3**. In the step **5**-**6** an aromatic ring is formed, and this can be the reason why the step is more exoergic than **2**-**4**. But in **5** the in plane lobes which are going to form the new σ bond belong to diverging triple bonds, while in **2** these are approximately parallel. The larger distortion necessary to attain the TS can offer an explanation of the **5**-**6** barrier being higher than **2**-**4** (Figure 1).

The kernel of the Bergman reaction[43] can again be recognized in the step **5**-**6** of Scheme 5. The main difference, as for the preceding model, is the substitution of a C–H bond with an unpaired electron. Though the Bergman cyclization produces a *p*-benzyne structure, here the already present unpaired electron brings about the formation of a couple of two adjacent radical lobes too. Once more, a situation recalling locally *o*-benzyne is obtained. The quartet-doublet energy difference in **6** is 45.6 kcal mol^{-1}, and indicates again that some bonding is present. In fact, **6** presents a situation closer to **4** than to **3**.

The bonding present in **6** entails some energy gain in correspondence of the cyclization **5**-**6**, which cannot obviously be attained in the Bergman reaction. A more favorable energy change upon cyclization step is found.

TABLE 4. Model system 2: CASPT2/CBS energy and "free energy"[a] differences.

	ΔE	ΔG /kcal mol^{-1}					
T/K:		*900*	*1200*	*1500*	*1800*	*2100*	*2400*
TS HCC + BD	66.7	58.8	56.9	55.1	53.4	51.9	50.4
TS H· + HT	67.6	56.3	53.3	50.5	47.8	45.2	42.6
5 (A)	0.0	0.0	0.0	0.0	0.0	0.0	0.0
TS **5**-**6**	30.3	38.9	42.8	46.7	50.8	55.0	59.2
6	-18.1	-3.0	1.9	6.9	11.9	16.9	21.9

[a]CASPT2/CBS energies combined with CASSCF/cc-pvTZ vibrational analysis.

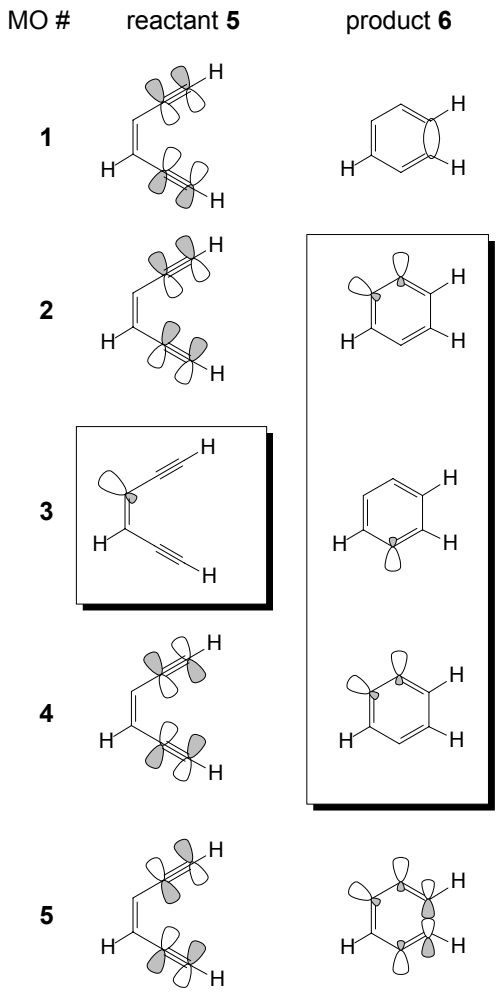

Scheme 6. Active orbitals for Model system 2. Boxes collect orbitals with electron occupations which deviate to a different extent from 2 or 0 (compare data in Table 5), related to the presence of unpaired electrons.

Scheme 6 can be useful in reading the data of Table 5. As for Model 1, it introduces schematically the characteristics of the active MOs, on the basis of which the electron configurations are defined. Inspection of Table 5 shows (bold figures) that some limited diradical character is present in the TS **5**-**6**, and then in **6**, though to a lesser extent (γ_i: 1.739-1.782 and 0.261-0.216, for TS **5**-**6** and **6**, respectively). This trait is present, notwithstanding

the significant overlap between the two adjacent lobes, which brings about the singlet – triplet splitting just discussed. These features can be compared again with the similar structures in the Bergman reaction. The weight of the most important configuration reflects the same trends (0.89-0.94 vs 0.90-0.77).

TABLE 5. Comparison of the wavefunction features for the ring closure step in model system 2.

	5	TS **5-6**	**6**
Active MO #	One-electron symbolic density matrix diagonal elements γ_i		
1	1.944	1.928	1.990
2	1.933	**1.750**	**1.796**
3	*1.001*	*1.001*	*1.002*
4	0.067	**0.251**	**0.201**
5	0.056	0.071	0.010
CF	Largest CAS(5,5)[a] CI coefficients:[b]		
$\mathbf{1^2\ 2^2\ 3^1}$	0.962	0.887	0.941
$\mathbf{1^2\ 3^1\ 4^2}$	0.161	0.232	0.300
$\mathbf{1^2\ 2^1\ 3^1\ 4^1}$		-0.262	

[a]active space encompassing one sp^2 hybrid associated to one unpaired electron (γ_i values in italic), plus the "reactant" in-plane π, π^* couples involved in the formation of the "product" σ bond and of the two sp^2 hybrids electron occupations differing more or less significantly from 2 or 0, related to the presence of new "unpaired" electrons (γ_i: bold values). See text and Scheme 5 for details.
[b]values larger than 0.15 reported.

Model 3. Finally, a system that could originate from the attack of propargyl to BD was explored (Scheme 7).

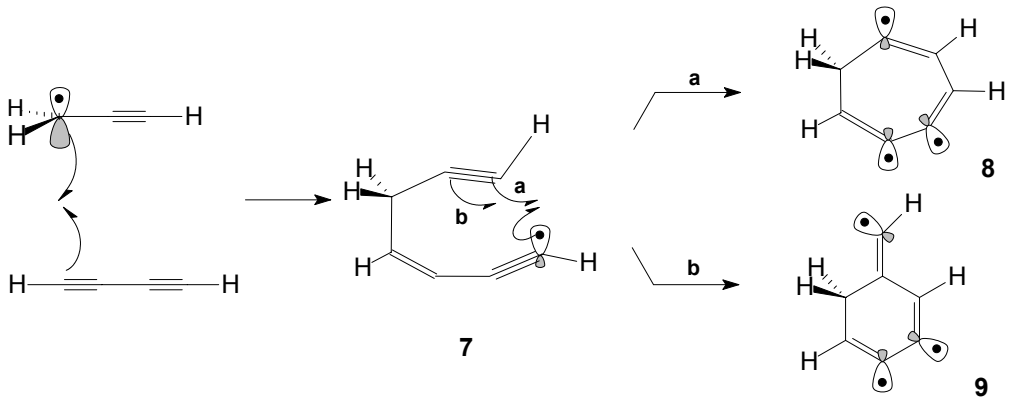

Scheme 7. Model system 3 (propargyl + butadiyne, BD) of the radical center proliferation mechanism for PAH growth (see Table 6).

The adduct **7** can close to a 7-ring (path **a**) or to a 6-ring (path **b**). Both cyclizations imply the formation of distant in-plane unpaired electrons, but the presence, already in **7**, of one unpaired electron creates a situation similar to those already seen before, in which the spin pairing in an "o-benzyne-like" electron couple forces the doublet multiplicity. Two possible ring closures are considered, leading to the cyclic structures **8** and **9**. The step is slightly endoergic (ΔE) in the former case, much more so in the latter.

TABLE 6. Model system 3: CASPT2/CBS energy and "free energy"[a] differences.

	ΔE	ΔG /kcal mol^{-1}					
T/K:		*900*	*1200*	*1500*	*1800*	*2100*	*2400*
HCCC·H_2 + BD	33.6	26.1	24.5	23.0	21.6	20.3	19.0
7 (A)	0.0	0.0	0.0	0.0	0.0	0.0	0.0
TS **7**-**8**	28.6	37.9	41.9	46.0	50.2	54.5	58.9
8	3.8	18.7	23.5	28.4	33.3	38.2	43.1
TS **7**-**9**	36.6	45.1	48.9	52.7	56.7	60.8	64.9
9	22.2	34.1	38.0	42.0	45.9	49.9	53.9

[a]CASPT2/CBS energies combined with CASSCF/cc-pvTZ vibrational analysis.

The barriers vary accordingly (Figure 1). The ΔG variation in the T = 900–2400 K range corresponds to a barrier increase of ca. 20 kcal mol^{-1} in both cases. Both **8** and **9** contain a saturated carbon, because of the propargylic methylene group.Therefore, neither cyclic structure has electronic features implying some energy gain (as in 6), apt to face the destabilization caused by the overall disruption of one electron pair (the situation attained in **8** and **9** resembles that in **4**). Besides, as in **4** and **6**, it does not seem that an authentic proliferation of radical centers can take place in this model. Indeed, the CASPT2/CBS energy differences between the ground state doublet and the corresponding quartet in **8** and **9** are 50.2 and 35.5 kcal mol^{-1}, respectively.

Scheme 8 can be helpful in reading the data of Table 7. Again, it introduces schematically the characteristics of the active MOs, on the basis of which the electron configurations are built. Inspection of Table 7 shows that, proceeding from TS **7**-**8** to **8**, very little diradical character is present. The two active-MO populations which could indicate diradical character are γ_i = 1.83-1.86 and 0.17-0.14, in TS **7**-**8** and **8**, respectively. Then, the largest c_i in Ψ is larger than 0.9, actually larger in **8** than in the preceding TS. Then a slightly more pronounced diradical character is seen in correspondence of TS **7**-**9**. But the coupling between the two adjacent lobes seems to be efficient in both cyclic structures, very slightly less so in **9**. These features are consistent with the large energy differences between the doublet and the quartet found for **8** and **9**.

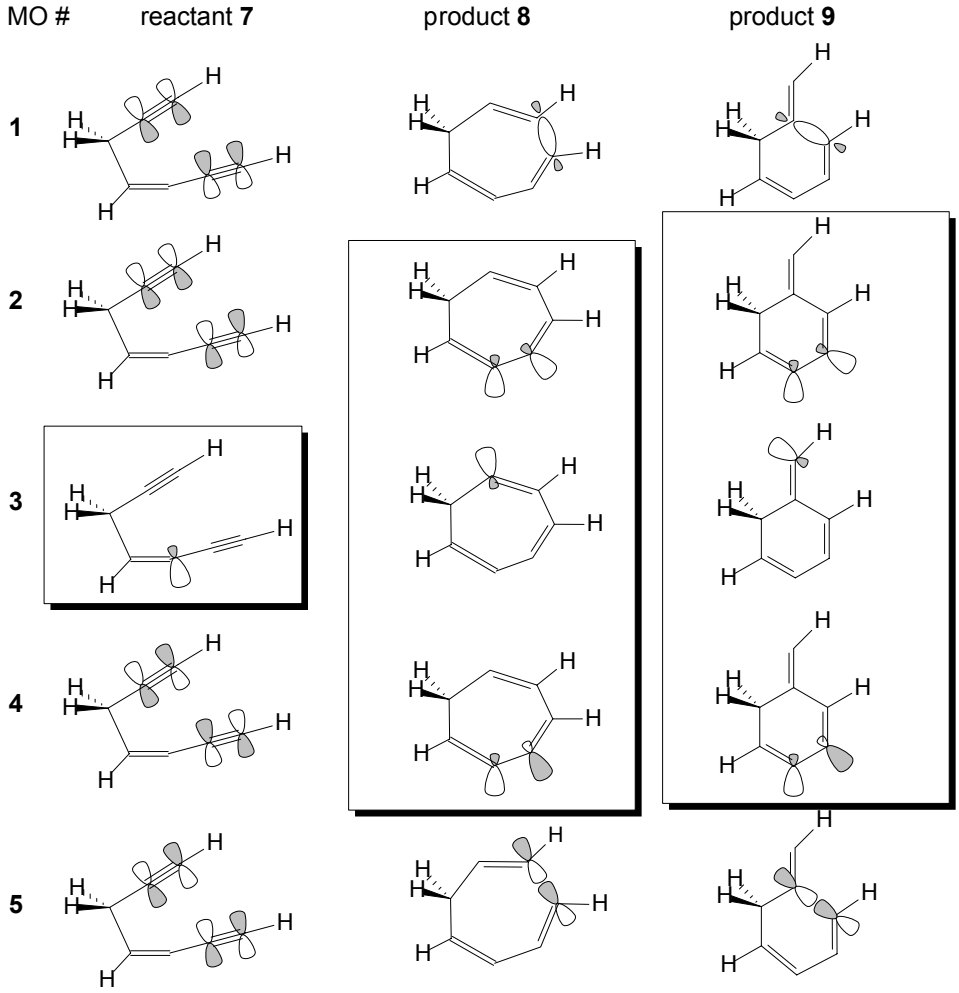

Scheme 8. Active orbitals for Model system 3 (compare data in Table 7). Boxes collect orbitals with electron occupations differing more or less significantly from 2 or 0, related to the presence of unpaired electrons.

TABLE 7. Wavefunction features for the ring closure step in model system 3.

	7	TS **7**-**8**	**8**	TS **7**-**9**	**9**
Active MO #	One-electron symbolic density matrix diagonal elements γ_i				
1	1.945	1.924	1.985	1.940	1.984
2	1.932	**1.830**	**1.859**	**1.752**	**1.786**
3	*1.001*	*1.002*	*1.000*	*1.000*	*1.000*
4	0.067	**0.168**	**0.141**	**0.250**	**0.214**
5	0.055	0.075	0.015	0.058	0.016
CF		Largest CAS(5,5)[a] CI coefficients:[b]			
$1^2\ 2^2\ 3^1$	0.962	**0.914**	**0.960**	**0.886**	**0.940**
$1^2\ 3^1\ 4^2$	0.151	0.178	0.264	0.225	0.321
$1^2\ 2^1\ 3^1\ 4^1$ [c]		0.208		0.290	
$1^2\ 2^1\ 3^1\ 4^1$ [c]				0.167	

[a] Active space encompassing one sp^2 hybrid associated to one unpaired electron (γ_i values in italic), plus the "reactant" in-plane π, π^* couples involved in the formation of the "product" σ bond and of the two sp^2 hybrids electron occupations differing more or less significantly from 2 or 0, related to the presence of new "unpaired" electrons (γ_i: bold values). See text and Scheme 5 for details. [b] Values larger than 0.15 reported. [c] The two configurations differ in the spin of the singly occupied MOs.

In the three models of cyclization-radical breeding step, the more or less pronounced energy minima (stable intermediates) are related to the initial open-chain intermediates A (**2**, **5**, and **7**) and to the "products" B (**3** or **4**, **6**, and **8** or **9**). In particular, it is apparent (Figure 1) that in Model 1 only the minima corresponding to **2** and **4** could be populated significantly. In fact, **3** faces a tiny *E* barrier for the backwards step to **2** (which could be barrierless even in terms of *G*).

Since the key step, cyclization accompanied by radical breeding, is a process based on the *disruption of electron pairs*, it is not surprise that it is an *energy demanding stage*. In fact, $\Delta E^{\ddagger}_{CASPT2}$ = 35 (step **2**-**3**), 27 (step **2**-**4**), 30 (step **5**-**6**), 29 (step **7**-**8**), and 37 (step **7**-**9**) kcal mol^{-1}, for Models 1-3. However, every cyclization is preceded by an addition step, whose backwards barrier ΔE_A determines (as a first approximation) how much excess energy will be available to the adduct A in the subsequent unimolecular step. In all cases, but for the **7**-**9** step, this energy results larger than the cyclization barrier the system has to ovecome: ΔE_A = 45, 67-68, and 34 kcal mol^{-1}, for Models 1-3, with respect to the adduct.

Yet, it is the temperature dependence of the free energy barriers that has to be inspected and taken into account. Therefore, let us define the ΔG for the backwards barrier relevant to A formation step as ΔG_A. Its value will very roughly define the free energy available at different temperatures to the unthermalized system to overcome the cyclization barrier that follows, ΔG_{cyc}. Upon inspection of Figure 2, it is apparent that the balance between ΔG_A and ΔG_{cyc}

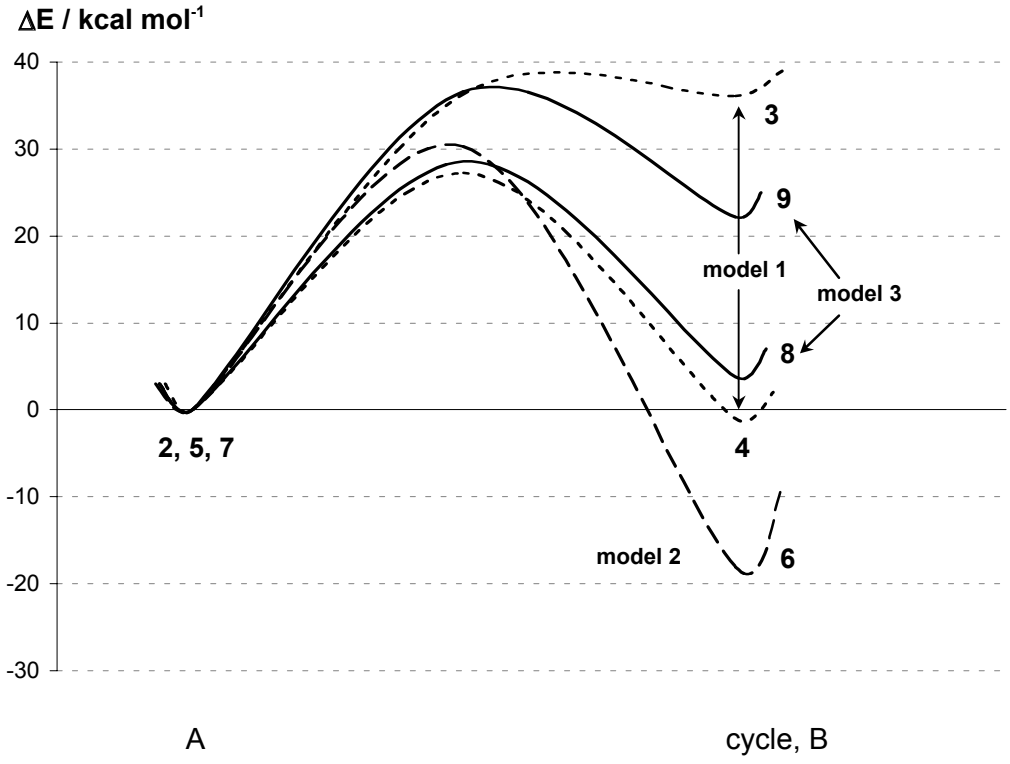

Figure 1. The CASPT2/CBS energy profiles for the “cyclization-radical proliferation” step. Model 1: steps **2**-**3** and **2**-**4** (dashed lines). Model 2: step **5**-**6** (longer dashes). Model 3: steps **7**-**8** and **7**-**9** (continuous lines). Points **2**, **5**, and **7** are arbitrarily set to the same energy.

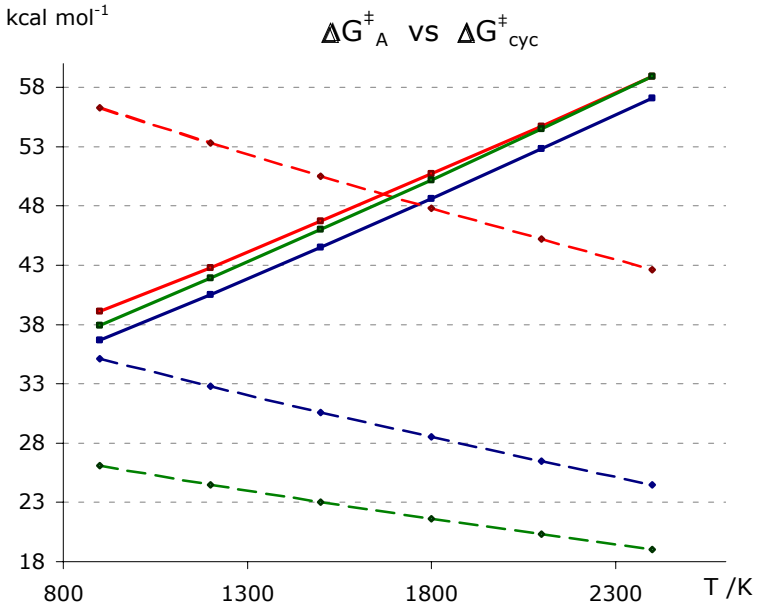

Figure 2. The free energy balance between what is available as a consequence of the formation of A (**2**, **5**, or **7**: dashed lines) and the barrier for the cyclization and radical breeding (steps **2**-**4**, **5**-**6**, or **7**-**8**: continuous lines**.** Blue: Model 1; red: Model 2; green: Model 3. For Models 1 and 3 only the data for the preferred cyclization mode are shown.

becomes less favourable to the cyclization-radical proliferation process upon T increase. On one hand, as expected, the -TΔS term penalizes the cyclization step (continuous lines). On the other hand, for the same reason, the formation of A is related to a reverse barrier which decreases with increasing temperature (dashed lines).

From this point of view, Model 1 (see Figure 2, blue lines) would seem hardly viable, since the two *G* maxima are comparable already at 900 K: ΔG_A = 35.1 (formation of **4**) vs ΔG_{cyc} = 36.7 kcal mol^{-1}. The comparison becomes more and more unfavourable as we proceed to higher temperatures. For Model 2 (see Figure 3, red lines) a crossing occurs between T = 1500 and T = 1800 K: ΔG_A = 50.5 (formation of **6**) vs ΔG_{cyc} = 46.7 kcal mol^{-1} becomes 47.8 vs 50.7. Hence, this process could be seen as possibly practicable only up to some intermediate combustion temperatures (ca. 1600 K). As regards Model 3 (see Figure 3, green lines) the situation appears to be the less promising, because the energy supposedly available from the A formation step is smaller than that required to cyclize right from the lowest temperature.

CONCLUSIONS

Radical attacks onto simple polyynes [(1) $H^{\bullet}$ + C_4H_2 + C_4H_2; (2) $H^{\bullet}$ + C_6H_2 or $HCC^{\bullet}$ + C_4H_2; with equivalent outcome; (3) $CH_2^{\bullet}CCH$ + C_4H_2] have been considered, which can generate open-chain radical intermediates, collectively labeled as A (structures **2**, **5**, or **7**). A, in all cases, can undergo a particular cyclization to B, apt to cause proliferation of radical centers. The focus of this CASPT2 and CASSCF study is on the key step "A $\rightarrow$ cycle B" in the polyyne-based “radical breeding mechanism” for PAH growth, proposed by Krestinin.

The electronic features of these cyclizations, discussed by analyzing some attributes of the multiconfiguration wavefunction, indicate that cyclization transition structures and cyclized products B show some sort of triradical character, present to a variable extent. It corresponds to the existence of the unpaired electron already present in A, plus two (spin-paired) electrons generated in the cyclization step. However, in most B cases one of these new singly occupied sp^2 orbitals is adjacent to the unpaired electron lobe already existent in A. This “ortho-like” position brings about a significant overlap and some sort of bonding. The triradical character is consequently reduced in a significant way.

The cyclization barriers (ΔG_{cyc}) of the open-chain intermediates A may be compared with the free energy drop (ΔG_A) which accompanies A formation. ΔG_A can be very approximately thought of as the amount of free energy available to surmount to cyclization barrier if A is unthermalized. The free energy balance between ΔG_A and ΔG_{cyc} shows the expected unfavorable dependence on the temperature (Figure 2). Only Model 2 seems to be indicative of a possible role of the radical breeding mechanism during combustion.

APPENDIX

Here, the choice of the active space selected in this study is briefly justified on the basis of the energy results collected in Table 8. The cyclization process recalls basically the Bergman reaction (Scheme 2) for all models. Therefore, we have tested on this reaction the following choices. (a) The one adopted for this study, and presented in the Method section, which corresponds (for the Bergman cyclization) to a CAS (4,4) for both CASSCF geometry optimizations and the ensuing PT2 refinement of the energy by single-point calculations. The active space is then further extended by adding the (6,6) contribution of the π system orthogonal to the molecular plane, to explore if its inclusion can affect the energetics significantly. The CAS (10,10) so obtained can be either used only for the PT2 computation carried out on the (4,4) geometry, (b), or in both phases, i.e. also in the preceding CASSCF optimization (c). These choices define a first set of test computations (Set 1). A second set of calculations consists in performing numerical CASPT2 optimizations right from the beginning, thus skipping the CASSCF phase. The information provided is obviously about the possible role of the geometry in affecting the energetics. This approach was not adopted in the present study, but can provide here a further set of reference values (Set 2).

TABLE 8. The Bergman reaction: Test of different CAS choices on the reaction energetics[a].

	TS	product
Set 1[b]		
(a) CAS(4,4)PT2//CAS(4,4)SCF (this work)	24.8	4.0
(b) CAS(10,10)PT2//CAS(4,4)SCF	25.9	4.8
(c) CAS(10,10)PT2//CAS(10,10)SCF	25.2	5.7
Set 2[c]		
CAS(4,4)PT2//CAS(4,4)PT2	24.4	4.8
CAS(10,10)PT2//CAS(10,10)PT2	26.4	5.6

[a] CASPT2 energy differences, in kcal mol^{-1}, with respect to the reagent. The cc-pvTZ basis set is used throughout.
[b] energies obtained in correspondence of CASSCF optimizations.
[c] energies obtained in correspondence of numerical CASPT2 optimizations.

As can be see from the data belonging to Set 1, the variation in the ring closure barrier is not large. Neither the data under the label (a) in Set 1 are far from the “best reference” provided by Set 2.

Acknowledgment. This work was conducted in the frame of EC FP6 NoE ACCENT (Atmospheric Composition Change, the European NeTwork of Excellence). One grant from Regione Piemonte has supported the Ph. D. bursary of A. G., and a second funding by Regione Piemonte supports both the Ph. D. bursary of A. I. and the present research work [DD n. 1 (18.1.2006); DD. n. 64 (2.12.2005); Bando Ricerca Scientifica - Settore *Sviluppo Sostenibile*]. Helpful duscussions with Dr. Andrea Maranzana are acknowledged.

Supplementary Material. A pdf file includes the energies and geometries of all optimized structures and MO plots for all transition structures. It is freely available in Wiley Interscience.

REFERENCES

(1) W.F. Cooke, J.J.N. Wilson, *J. Geophys. Res.* **1996**, *101*, 19395-19409. C. Liousse, J.E. Penner, C. Chuang, J.J. Walton, H. Eddleman, H. Cachier, *J. Geophys. Res.* **1996**, *101*, 19411-19432.

(2) B.J. Finlayson-Pitts, J.N. Pitts, Jr., *Chemistry of the Upper and Lower Atmosphere*; Academic Press: New York, **2000**; Chapters 9 and 10.

(3) M. Pilar Ruiz, R. Guzmán de Villoria, Á. Millera, M.U. Alzueta, R. Bilbao, *Ind. Eng. Chem. Res*. **2007**, *46*, 7550-7560.

(4) K.-H. Homann, *Angew. Chem. Int. Ed.* **1998**, *37*, 2435-2451.

(5) P.A. Vlasov, J. Warnatz, *Proc. Comb. Inst.* **2002**, *29*, 2335-2341;

(6) See for instance: L. Liu, K.T. Rim, D. Eom, T.F. Heinz, G.W. Flynn, *Nano Lett.* **2008**, *8*, 1872-1878. C.H. Kim, F. Xu, G.M. Faeth, *Comb. Flame.* **2008**, *152*, 301-316. Y. Kobayashi, T. Furuhata, K. Amagai, M. Arai, *Comb. Flame.* **2008**, *154*, 346-355. A. Yozgatligil, M.R. Zachariah, *Comb. Sci. Tech.* **2008**, *180*, 941-949. A. D'Anna, *Energy & Fuels* **2008**, *22*, 1610-1619.

(7) E.H. Wilson, S.K. Atreya, *Planet. Space Sci.* **2003**, *51*, 1017-1033.

(8) I. Cherchneff, J.R. Barker, A.G.G.M. Tielens, *Astrophys. J.* **1991**, *377*, 541-552. J. Cernicaro, A.M. Heras, J.R. Pardo, A.G.G.M. Tielens, M. Guélin, E. Dartois, R. Neri, L.B.F.M. Waters, *Astrophys. J.* **2001**, 546, L127-L130. J. Cernicaro, *Astrophys. J.* **2004**, 608, L41-L44.

(9) L.J. Allamandola, A.G.G.M. Tielens, J.R. Barker, *Astrophys. J. Suppl. Series* **1989**, *71*, 733-775.

(10) M. Frenklack, *Phys. Chem. Chem. Phys.* **2002**, *4*, 2028-2037.

(11) I. Cherchneff, J.R. Barker, A.G.G.M. Tielens, *Astrophys. J.* **1992**, *401*, 269-287; *ibidem* **1993**, *413*, 445, erratum.

(12) M. Frenklach, D.W. Clary, W.C. Gardiner, S.E. Stein, *Proc. Combust. Inst.* **1985**, *20*, 887-901.

(13) H. Bockhorn, F. Fetting, H.W. Wenz, *Ber. Bunsen-Ges. Phys. Chem.* **1983**, *97*, 1067-1073.

(14) J.D. Bittner, J.B. Howard, *Symp. Int. Combust. Inst.* **1981**, *18*, 1105-1116.

(15) H. Richter, J.B. Howard, *Progr. En. Combust. Sci.* **2000**, *26*, 565-608.

(16) C.W. Bauschlicher, Jr., A. Ricca, *Chem. Phys. Lett.* **2000**, *326*, 283-287.

(17) H. Richter, O.A. Mazyar, R. Sumathi, W.H. Green, J.B. Howard, J.W. Bozzelli, *J. Phys. Chem. A* **2001**, *105*, 1561-1573.

(18) V.V. Kislov, N.I. Islamova, A.M. Kolker, S.H. Lin, A.M. Mebel, *J. Chem. Theory. Comput.* **2005**, *1*, 908-924.

(19) See for instance: N.M.; Marinov, W.J. Pitz, C. K. Westbrook, A.M. Vincitore, M.J. Castaldi, S.M. Senkan, C. F. Melius, *Combust. Flame* **1998**, *114*, 192-213.

(20) A.V. Krestinin, *Combust. Flame* **2000**, *121*, 513-524. A.V. Krestinin, *Chem. Phys. Rep.* **1998**, *17*, 1441-1461. A.V. Krestinin, *Chem. Phys. Rep.* **1994**, *13*, 191-210.

(21) W.W. Duley, *Astrophys. J.* **2000**, 528, 841-848. H.W. Kroto, J.R. Heath, S.C. O'Brien, R.F. Curl, R.E. Smalley, *Astrophys. J.* **1987**, 314, 352-355. I.W.M. Smith, A.M. Sage, N.M. Donahue, E. Herbst , D. Quan, *Faraday Discuss.* **2006** 133 137-156.

(22) F. Goulay, D.L. Osborn, C.A. Taatjes, P. Zou, G. Meloni, S.R. Leone, *Phys. Chem. Chem Phys*. **2007**, *9*, 4291-4300.

(23) N. Hansen, S.J. Klippenstein, P.R. Westmoreland, T. Kasper, K. Kohse-Höinghaus, J. Wang, T.A. Cool, *Phys. Chem. Chem. Phys.* **2008**, *10*, 366.374.

(24) H. Li, L. Zhang, Z. Tian, T. Yuan, K. Zhang, B. Yang, F. Qi, *Proc. Comb. Inst.* **2009**, **32**, 1293-1300.

(25) J.Z. Wen, M.J. Thomson, M.F. Lightstone, S.N. Rogak, *Energy & Fuels* **2006**, *20*, 547-559.

(26) (a) B. Yang, Y. Li, L. Wei, C. Huang, J. Wang, Z. Tian, R. Yang, L. Sheng, Y. Zhang, F. Qi, *Proc. Comb. Inst.* **2007**, *31*, 555–563.

(27) Y. Li, C. Huang, L. Wie, B. Yang, J. Wang, Z. Tian, T. Zhang, L. Sheng, F. Qi, *Energy & Fuels* **2007**, 1931-1941.

(28) J. Warnatz, *Comb. Sci. Tech.* **1983**, *34*, 177-200. J. Warnatz, *Ber. Bunsen. Phys. Chem.* **1983**, *87*, 1008-1022.

(29) Y. Hidaka, Y. Henmi, T. Ohonishi, T. Okuno, T. Koike, *Comb. & Flame* **2002**, *130*, 62-82.

(30) Molar fractions X were assessed in flames of ethyne (ref. 24), benzene (ref. 26), and gasoline (ref. 27), as reported below:

	$C_2H_2/O_2/Ar$	$C_6H_6/O_2/Ar$	gasoline/O_2/Ar
ethyne	-	2.4×10^{-2}	-
butadiyne	4.4×10^{-3}	6.3×10^{-3}	4.4×10^{-3}
hexatriyne	-	1×10^{-3}	8×10^{-4}
ethynyl	-	2.4×10^{-5}	-
propargyl	2.4×10^{-3}	2.4×10^{-3}	2.4×10^{-3}

(31) (a) P.-Å. Malmqvist, A. Rendell, B.O. Roos, *J. Phys. Chem.*, **1990**, *94*, 5477-5482. B.O. Roos, P.R. Taylor, P.E.M. Siegbahn, *Chem. Phys.* **1980**, *48*, 157-173. B.O. Roos, "The complete active space self-consistent field method and its applications in electronic structure calculations", in *Advances in Chemical Physics - Ab Initio Methods in Quantum Chemistry II*, chapter 69, p 399 (Editor: K.P. Lawley); John Wiley & Sons Ltd., Chichester, England, **1987**. ISBN: 0-470-14294-4. (b) The implementation of this kind of approach in the Gaussian program system is documented in: D. Hegarty, M.A. Robb, *Mol. Phys.* **1979**, *38*,1795-1812 and R.H.A. Eade, M.A. Robb, *Chem. Phys. Lett.* **1981**, *83*, 362-368.

(32) (a) Sketches of MOs are drawn by using CHEMWINDOW 6.0, BioRad laboratories, Sadtler Division, Philadelphia, USA. (b) Actual MO plots are genereted by MOLDEN: G. Schaftenaar and J. H. Noordik, *J. Comput.-Aided Mol. Design* **2000**, **14**, 123-134, whose web site is: http://www.cmbi.ru.nl/molden/molden.html.

(33) cc-pvTZ: R.A. Kendall, T.H. Dunning Jr., R.J. Harrison, *J. Chem. Phys.* **1992**, *96*, 6796. cc-pvQZ: D.E. Woon, T.H. Dunning Jr., *J. Chem. Phys.* **1995**, *103*, 4572.

(34) K. Andersson, P.-Å. Malmqvist, B.O. Roos, A.J. Sadley, K. Wolinski, *J. Phys. Chem.* **1990**, *94*, 5483 -5488. K. Andersson, P.-Å. Malmqvist, B.O. Roos, *J. Phys. Chem.* **1992**, *96*, 1218-1226.

(35) G. Ghigo, B.O. Roos, P.-Å. Malmqvist, *Chem. Phys. Lett.* **2004**, *396*, 142-149.

(36) A. Halkier, T. Helgaker, P. Jørgensen, W. Klopper, H. Koch, J. Olsen, A. K. Wilson, *Chem. Phys. Lett.* **1998**, 286, 243-252.

(37) B. Foresman, Æ. Frisch, *Exploring Chemistry with Electronic Structure Methods*, Gaussian, inc., Pittsburgh, PA (USA), **1996**, 166-168 (ISBN 0-9636769-3-8).

(38) Gaussian 03, Revision B.05, M.J. Frisch, G.W. Trucks, H.B. Schlegel, G.E. Scuseria, M.A. Robb, J.R. Cheeseman, J.A. Montgomery, Jr., T. Vreven, K.N. Kudin, J.C. Burant, J.M. Millam, S.S. Iyengar, J. Tomasi, V. Barone, B. Mennucci, M. Cossi, G. Scalmani, N. Rega, G.A. Petersson, H. Nakatsuji, M. Hada, M. Ehara, K. Toyota, R. Fukuda, J. Hasegawa, M. Ishida, T. Nakajima, Y. Honda, O. Kitao, H. Nakai, M. Klene, X. Li, J.E. Knox, H.P. Hratchian, J.B. Cross, V. Bakken, C. Adamo, J. Jaramillo, R. Gomperts, R.E. Stratmann, O. Yazyev, A.J. Austin, R.

Cammi, C. Pomelli, J.W. Ochterski, P.Y. Ayala, K. Morokuma, G.A. Voth, P. Salvador, J.J. Dannenberg, V.G. Zakrzewski, S. Dapprich, A.D. Daniels, M.C. Strain, O. Farkas, D.K. Malick, A. D. Rabuck, K. Raghavachari, J.B. Foresman, J.V. Ortiz, Q. Cui, A.G. Baboul, S. Clifford, J. Cioslowski, B.B. Stefanov, G. Liu, A. Liashenko, P. Piskorz, I. Komaromi, R.L. Martin, D.J. Fox, T. Keith, M.A. Al-Laham, C.Y. Peng, A. Nanayakkara, M. Challacombe, P.M.W. Gill, B. Johnson, W. Chen, M.W. Wong, C. Gonzalez, and J.A. Pople, Gaussian, Inc., Wallingford CT, **2004**.

(39) G. Karlström, R. Lindh, P.-Å. Malmqvist, B.O. Roos, U. Ryde, V. Veryazov, P.-O. Widmark, M. Cossi, B. Schimmelpfennig, P. Neogrady, L. Seijo, *Computational Material Science* **2003**, *28*, 222-239.

(40) (a) Molcas, release 7.2. K. Andersson, F. Aquilante, M. Barysz, E. Bednarz, A. Bernhardsson, M.R.A. Blomberg, Y. Carissan, D.L. Cooper, M. Cossi, A. Devarajan, L. De Vico, N. Ferré, M.P. Fülscher, A. Gaenko, L. Gagliardi, G. Ghigo, C. de Graaf, B.A. Hess, D. Hagberg, A. Holt, G. Karlström, J.W. Krogh, R. Lindh, P.-Å. Malmqvist, T. Nakajima, P. Neogrády, J. Olsen, T.B. Pedersen, J. Raab, M. Reiher, B.O. Roos, U. Ryde, B. Schimmelpfennig, M. Schütz, L. Seijo, L. Serrano-Andrés, P.E.M. Siegbahn, J. Stålring, T. Thorsteinsson, V. Veryazov, P.-O. Widmark, and A. Wolf, Department of Theoretical Chemistry, Lund University, Sweden (2008). (b) F. Aquilante, L. De Vico, N. Ferré, G. Ghigo, P.-Å. Malmqvist, P. Neogrády, T.B. Pedersen, M. Pitoňák, M. Reiher, B.O. Roos, L. Serrano-Andrés, M. Urban, V. Veryazov, R. Lindh, "*MOLCAS 7: The Next Generation*" *J. Comput. Chem.* **2009**, in the press.

(41) The experimental energy splitting between the ground state singlet and the corresponding triplet in *o*-benzyne is large, 37-38 kcal mol^{-1} (while it is measured as - -3.8 kcal mol^{-1} for *p*-benzyne: P.G. Wenthold, R.R. Squires, W.C. Lineberger, J. Am. Chem. Soc. **1998**, *120*, 5279-5290).

(42) See discussion in: K.K. Thoen, H.I. Kenttämaa, *J. Am. Chem. Soc*. **1999**, *121*, 800-805. S. Yamabe, T. Minato, A. Ishiwata, O. Irinamihira, T. Machiguchi, *J. Org. Chem.,* **2007**, 72, 2832 -2841.

(43) R.R. Jones, R.G. Bergman, *J. Am. Chem. Soc*. **1972**, *94*, 660-661. R.G. Bergman, *Acc. Chem. Res.* **1973**, *6*, 25-31.

(44) The Bergman reaction has an experimentally assessed enthalpy barrier of 32 kcal mol^{-1}, which corresponds to a step enthalpy of 8-13 kcal mol^{-1}.

(45) E. Kraka, D. Cremer, *J. Am. Chem. Soc.* **1994**, *116*, 4929-4936.

(46) R. Lindh, T.J. Lee, A. Berhardsson, B. J. Persson, G. Karlström, *J. Am. Chem. Soc.* **1995**, *117*, 7186-7194.

(47) J. Gräfenstein, A.M. Hjerpe, E. Kraka, D. Cremer, *J. Phys. Chem. A* **2000**, *104*, 1748-1761. See also ref. 9 therein.

(48) As regards the γ_i's ,values of ca. 1.9x and 0.0x (x=1-9) are related to the forming or formed σ bond, and represent the populations of one σ and one σ^* orbitals. A value close to 1 is related to a hybrid orbital, which carries one unpaired electron. By examining another couple of orbitals and reading, for instance, populations of 1.3 and 0.7, or 1.6 and 0.4, a more or less pronounced diradical character can be inferred. Just to provide a reference, in the *edge-to-edge* planar conformation of the diradical trimethylene ($CH_2CH_2CH_2$) the overlap S_{12} between the terminal-C p atomic orbitals is quite modest, but not zero. In this case, the largest CI coefficients for an active space (2,2) are $c_1 = 0.7380$, $c_2 = -0.6748$, and $\gamma_1 = 1.089$, $\gamma_2 = 0.911$. As a limiting case, the edge-to-face conformation, in which $S_{12}=0$, has $c_1 = 0.7071$ and $c_2 = -0.7071$ (i.e. $\pm 2^{-1/2}$), while $\gamma_1 = 1.000$ and $\gamma_2 = 1.000$.

(49) In a qualitatively consistent way, the singlet-triplet energy gap is in this case estimated at CAS(4,4)/cc-pvTZ to be just 0.9 kcal mol^{-1}.

(50) The symmetry of *p*-benzyne would suggest the use of a (6,6) active space. CAS(4,4) is chosen in view of the comparison with the (5,5) space of models 1-3.

TABLES

TABLE 1. Model system 1: CASPT2/CBS energy[a] and "free energy" [b] differences.

	ΔE	ΔG /kcal mol^{-1}					
T/K:		*900*	*1200*	*1500*	*1800*	*2100*	*2400*
add. TS **1**-**2**	44.8	35.1	32.8	30.6	28.5	26.5	24.5
2 (A)	0.0	0.0	0.0	0.0	0.0	0.0	0.0
TS **2**-**3**	34.1	44.4	48.6	53.0	57.6	62.2	66.9
	36.3	*46.6*	*50.8*	*55.3*	*59.8*	*64.4*	*69.1*
3	36.1	49.0	53.3	57.7	62.1	66.4	70.8
TS **2**-**4**	27.3	35.9	39.7	43.6	47.6	51.8	56.0
4	-1.0	13.4	18.1	22.9	27.6	32.4	37.2

[a]values in italic: point of maximum E for a CASPT2 scan (see Method section).
[b]CASPT2/CBS energies combined with CASSCF/cc-pvTZ vibrational analysis.

TABLE 2. Wavefunction features for the ring closure step in model system 1.

	2	TS **2**-**3**	**3**	TS **2**-**4**	**4**
Active MO #	One-electron symbolic density matrix diagonal elements γ_i				
1	1.945	1.954	1.983	1.922	1.985
2	1.931	**1.593**	**1.300**	**1.826**	**1.859**
3	*1.001*	*1.004*	*1.002*	*1.002*	*1.000*
4	0.068	**0.404**	**0.697**	**0.172**	**0.141**
5	0.056	0.045	0.017	0.076	0.015
CF		Largest CAS(5,5)[a] CI coefficients:[b]			
$\mathbf{1^2\ 2^2\ 3^1}$	0.961	**0.854**	**0.764**	0.912	0.960
$\mathbf{1^2\ 3^1\ 4^2}$		0.371	0.531		0.264
$\mathbf{2^2\ 3^1\ 5^2}$	0.152				
$\mathbf{1^2\ 2^1\ 3^1\ 4^1}$		-0.247	-0.273	0.214	
$\mathbf{1^2\ 2^1\ 3^1\ 5^1}$				0.177	

[a]active space encompassing one sp^2 hybrid associated to one unpaired electron (γ_i values in italic), plus the "reactant" in-plane π, π^* couples involved in the formation of the "product" σ bond and of the two sp^2 hybrids electron occupations differing more or less significantly from 2 or 0, related to the presence of new "unpaired" electrons (γ_i: bold values). See text and Scheme 3 for details.
[b]values larger than 0.15 reported.

TABLE 3. Comparison of the wavefunction features for the ring closure step in the Bergman reaction.

	Hexenediyne	ring closure TS	*p*-benzyne
Active MO #	One-electron symbolic density matrix diagonal elements γ_i		
1	1.942	1.937	1.989
2	1.945	**1.699**	**1.191**
3	0.056	**0.303**	**0.809**
4	0.057	0.060	0.011
CF	Largest CAS(4,4)[a] CI coefficients:[b]		
$\mathbf{1^2\ 2^2}$	0.972	0.906	**0.770**
$\mathbf{1^1\ 2^1\ 3^1\ 4^1}$	0.165	-0.170	
$\mathbf{1^2\ 3^2}$		-0.358	**-0.634**

[a] Active space as in models 1-3, minus the initial sp^2 hybrid associated to the unpaired electron in the starting radicals **2**, **5**, and **7**. See note 50, and the Supplemental Material for further details.

[b] values larger than 0.15 reported.

TABLE 4. Model system 2: CASPT2/CBS energy and "free energy"[a] differences.

	ΔE	ΔG /kcal mol^{-1}					
T/K:		*900*	*1200*	*1500*	*1800*	*2100*	*2400*
TS HCC + BD	66.7	58.8	56.9	55.1	53.4	51.9	50.4
TS H$^{\cdot}$ + HT	67.6	56.3	53.3	50.5	47.8	45.2	42.6
5 (A)	0.0	0.0	0.0	0.0	0.0	0.0	0.0
TS **5**-**6**	30.3	38.9	42.8	46.7	50.8	55.0	59.2
6	-18.1	-3.0	1.9	6.9	11.9	16.9	21.9

[a] CASPT2/CBS energies combined with CASSCF/cc-pvTZ vibrational analysis.

TABLE 5. Comparison of the wavefunction features for the ring closure step in model system 2.

5	TS **5**-**6**	**6**

Active MO #	One-electron symbolic density matrix diagonal elements γ_i		
1	1.944	1.928	1.990
2	1.933	**1.750**	**1.796**
3	*1.001*	*1.001*	*1.002*
4	0.067	**0.251**	**0.201**
5	0.056	0.071	0.010
CF	Largest CAS(5,5)[a] CI coefficients:[b]		
$\mathbf{1^2\ 2^2\ 3^1}$	0.962	0.887	0.941
$\mathbf{1^2\ 3^1\ 4^2}$	0.161	0.232	0.300
$\mathbf{1^2\ 2^1\ 3^1\ 4^1}$		-0.262	

[a]active space encompassing one sp^2 hybrid associated to one unpaired electron (γ_i values in italic), plus the "reactant" in-plane π, π^* couples involved in the formation of the "product" σ bond and of the two sp^2 hybrids electron occupations differing more or less significantly from 2 or 0, related to the presence of new "unpaired" electrons (γ_i: bold values). See text and Scheme 5 for details.

[b]values larger than 0.15 reported.

TABLE 6. Model system 3: CASPT2/CBS energy and "free energy"[a] differences.

	ΔE	ΔG /kcal mol^{-1}					
T/K:		*900*	*1200*	*1500*	*1800*	*2100*	*2400*
HCCC·H_2 + BD	33.6	26.1	24.5	23.0	21.6	20.3	19.0
7 (A)	0.0	0.0	0.0	0.0	0.0	0.0	0.0
TS **7**-**8**	28.6	37.9	41.9	46.0	50.2	54.5	58.9
8	3.8	18.7	23.5	28.4	33.3	38.2	43.1
TS **7**-**9**	36.6	45.1	48.9	52.7	56.7	60.8	64.9
9	22.2	34.1	38.0	42.0	45.9	49.9	53.9

[a]CASPT2/CBS energies combined with CASSCF/cc-pvTZ vibrational analysis.

Indeed, the CASPT2/CBS energy differences between the ground state doublet and the corresponding quartet in **8** and **9** are 50.2 and 35.5 kcal mol^{-1}, respectively.

TABLE 7. Wavefunction features for the ring closure step in model system 3.

	7	TS **7**-**8**	**8**	TS **7**-**9**	**9**
Active MO #	One-electron symbolic density matrix diagonal elements γ_i				

1	1.945	1.924	1.985	1.940	1.984
2	1.932	**1.830**	**1.859**	**1.752**	**1.786**
3	*1.001*	*1.002*	*1.000*	*1.000*	*1.000*
4	0.067	**0.168**	**0.141**	**0.250**	**0.214**
5	0.055	0.075	0.015	0.058	0.016
CF		Largest CAS(5,5)[a] CI coefficients:[b]			
$\mathbf{1^2\ 2^2\ 3^1}$	0.962	**0.914**	**0.960**	**0.886**	**0.940**
$\mathbf{1^2\ 3^1\ 4^2}$	0.151	0.178	0.264	0.225	0.321
$\mathbf{1^2\ 2^1\ 3^1\ 4^1}$ [c]		0.208		0.290	
$\mathbf{1^2\ 2^1\ 3^1\ 4^1}$ [c]				0.167	

[a] Active space encompassing one sp^2 hybrid associated to one unpaired electron (γ_i values in italic), plus the "reactant" in-plane π, π^* couples involved in the formation of the "product" σ bond and of the two sp^2 hybrids electron occupations differing more or less significantly from 2 or 0, related to the presence of new "unpaired" electrons (γ_i: bold values). See text and Scheme 5 for details.

[b] Values larger than 0.15 reported.

[c] The two configurations differ in the spin of the singly occupied MOs.